Inorganic Chemistry

Article

pubs.acs.org/IC

Carbene Generation by Cytochromes and Electronic Structure of Heme-Iron-Porphyrin-Carbene Complex: A Quantum Chemical Study

Nikhil Taxak, Bhargav Patel, and Prasad V. Bharatam*

Department of Medicinal Chemistry, National Institute of Pharmaceutical Education and Research (NIPER), S. A. S. Nagar (Mohali), 160 062 Punjab, India

Supporting Information

ABSTRACT: Carbene-heme-iron-porphyrin complexes generated from cytochrome P450 (CYP450)-mediated metabolism of compounds containing methylenedioxyphenyl (MDP) moiety lead to the mechanism-based inhibition (MBI) of CYPs. This coordination complex is termed as the metabolic-intermediate complex (MIC). The bioinorganic chemistry of MDP carbenes has been studied using quantum chemical methods employing density functional theory (B3LYP functional with implicit solvent corrections) to (i) analyze the characteristics of MDP-carbene in terms of singlet−triplet energy difference, protonation, and dimerization energies, etc.; (ii) determine the electronic structure and analyze the Fe-carbene interactions; and (iii) elucidate the potential reaction pathways for the generation of carbene, using **Cpd I** (iron(IV)-oxo-porphine with SH^- as the axial ligand) as the model oxidant to mimic the activity of CYP450. The results show that MDP-carbenes are sufficiently stable and nucleophilic, leading to the formation of stable MIC (−40.35 kcal/mol) on the doublet spin state, formed via interaction between σ_{LP} of carbene and empty d_{z^2} orbital of heme-iron. This was aided by the back-bonding between filled d_{xz} orbital of heme-iron and the empty p orbital of carbene. The mechanistic pathway proposed in the literature for the generation of MDP-carbene (CH hydroxylation followed by water elimination) was studied, and observed to be unfavorable, owing to the formation of highly stable hydroxylated product (−57.12 kcal/mol). An intriguing pathway involving hydride ion abstraction and proton transfer followed by water elimination step was observed to be the most probable pathway.

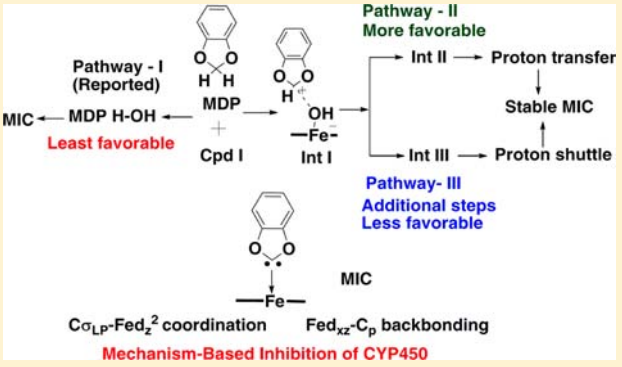

INTRODUCTION

Carbenes are known to form complexes with transition metals such as iron, ruthenium, palladium, gold, etc. These metal complexes are utilized as catalysts in organic and organometallic chemistry.[1−3] A plethora of carbene-metal complexes have been synthesized, involving the interactions between d-orbitals of metals and p-orbitals of carbenes.[4] Several theoretical studies employing density functional theory (DFT) have been carried out describing the electronic structure and geometries of carbene-metal complexes.[3] Frenking and co-workers have reported the comparison of carbon−ruthenium and carbon−iron complexes.[3] They also reported the electronic structure of complexes of N-heterocyclic carbenes (NHCs) with iron, osmium, ruthenium, and porphyrin.[3] Penka et al. discussed the bonding properties of NHCs coordinated to electron rich metal centers such as nickel, platinum, and palladium.[5] Carbenes are also being utilized in designing novel chemical species like divalent C(0) species and divalent N(I) species.[6] Thus, the inorganic chemistry of carbenes and their applications as catalysts in synthetic reactions has progressed significantly in the past few years.

The metal-carbene chemistry has also been reported to play an important role in biological systems. The iron-carbene complexes of porphyrins, azamacrocyclic ligands, etc. have been reported, wherein the in situ generated carbenes are complexed with iron.[7] Carbenes are also present naturally in biological conditions such as in the thiazolium moiety of thiamine pyrophosphate (TPP), vitamin B1 (thiamine) containing coenzyme, which catalyzes biochemical reactions such as glycolysis, protein, and carbohydrate biosynthesis.[8] Carbenes have also attracted interest in medicinal and therapeutic applications.[9] Thus, several theoretical and experimental studies highlight the inorganic, organic, and medicinal chemistry of carbenes.[1−9] However, the bioinorganic chemistry of carbenes and their implications in toxicity have not been explored thoroughly. Owing to their high nucleophilicity, carbenes show toxic effects in biological conditions. Specifically, the carbenes generated from cytochrome P450 (CYP450)-mediated metabolism of ligands containing methylenedioxyphenyl (MDP) group lead to the inhibition of CYP450 activity and further complications like drug−drug interactions and hepatotoxicity in the human body.[10]

Received: January 2, 2013
Published: April 5, 2013

   dx.doi.org/10.1021/ic400010d | *Inorg. Chem.* 2013, 52, 5097−5109

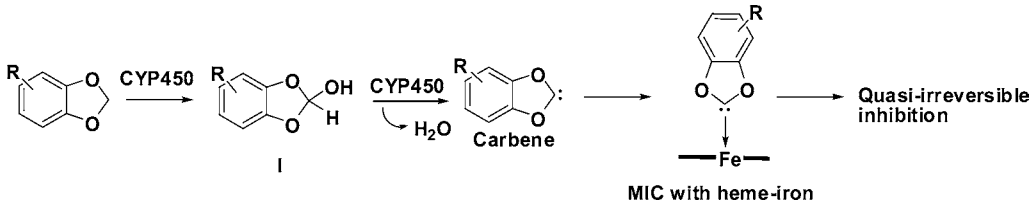

Figure 1. Suggested reaction pathway for the generation of reactive carbene species.

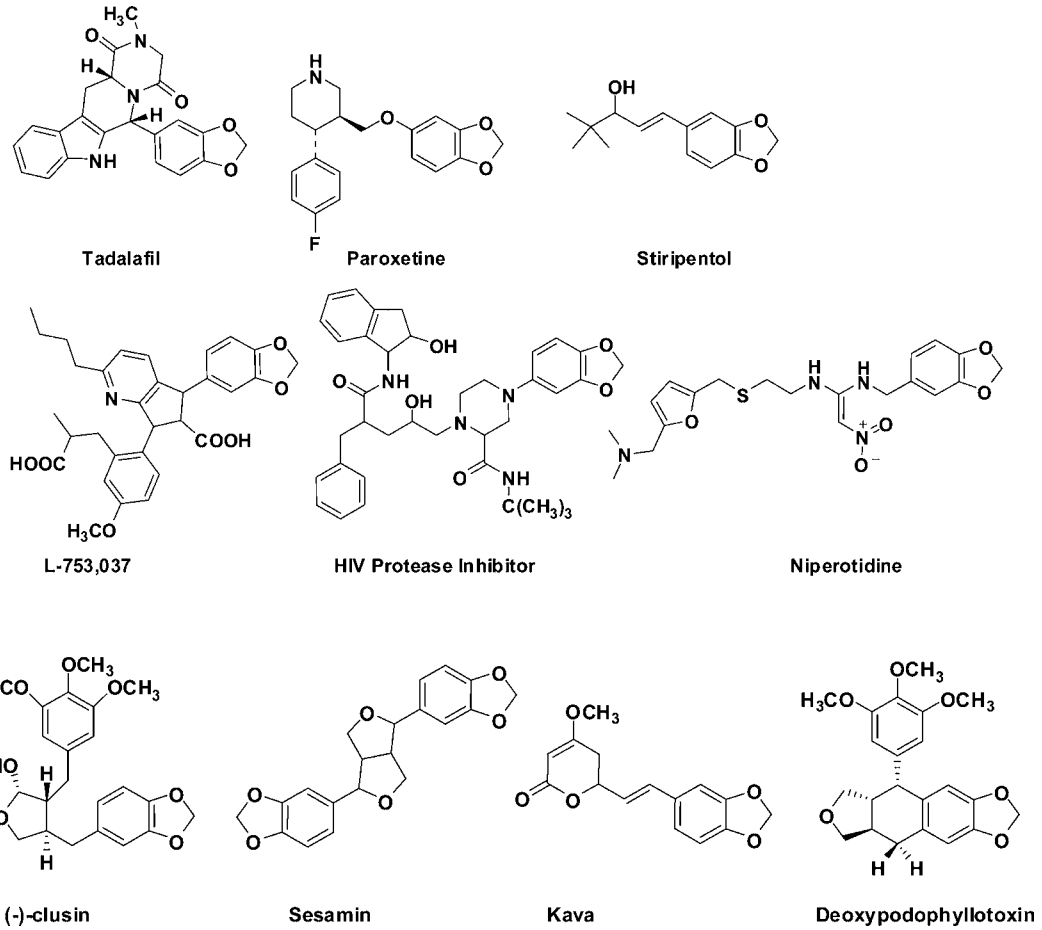

Figure 2. Structures of drugs and compounds under clinical evaluation containing MDP moiety and potentially leading to MBI of CYP450.

The MDP carbenes form a metabolic-intermediate complex (MIC) with the heme-iron via coordination, leading to quasi-irreversible inhibition of CYP450 (Figure 1).[11−22] Inhibition of cytochromes arising due to the reactive metabolite (RM) generated by the biotransformation of the substrate itself is known as the mechanism-based inhibition (MBI) of cytochromes.[22−28] The reactive species or RM is termed as the mechanism-based inhibitor which binds within the active site and interferes with the catalytic cycle of CYP450. MBI results in a more profound and prolonged effect as compared to reversible inhibitors, thus underlying its concern in drug metabolism.[10,23−28]

The MDP moiety forms an important constituent of several drugs, pesticides, flavoring agents, and naturally occurring compounds (Figure 2).[12−24] Drugs containing the MDP moiety which are reported to form the reactive carbene intermediate and MIC with heme-iron include tadalafil and paroxetine. Tadalafil, a selective phosphodiesterase-5 (PDE-5) inhibitor, has been reported to inhibit the activity of CYP3A4, via the formation of MIC between carbene intermediate and heme-iron.[12] Paroxetine, a selective serotonin reuptake inhibitor, acts as the potent inhibitor of CYP2D6 by forming an MIC of carbene-Fe.[13] Niperotidine is another example of a drug containing MDP moiety, which was withdrawn from the market owing to acute hepatitis.[14] The reactive metabolites via the oxidation of MDP unit have been implicated behind this toxicity;[14] however, no confirmatory reports are available in this regard.

Several compounds with MDP group have entered clinical and preclinical evaluation: stiripentol, an antiepileptic drug,[15] L-753,037, a potent endothelin (ET)-A and ET-B-receptor antagonist,[16] HIV protease inhibitor.[17] MDP lignans such as (−)-clusin, (−)-dihydroclusin, (−)-yatein, (−)-hinokinin, and (-)-dihydrocubebin, isolated from *Piper cubeba*, lead to inhibition of CYP3A4.[18] Sesamin and episesamin found in sesame oil and sesamin supplements contain two MDP moieties and lead to MBI, especially of CYP2C9.[19] Deoxypodophyllotoxin isolated from *Podophyllum peltatum*

dx.doi.org/10.1021/ic400010d | *Inorg. Chem.* 2013, 52, 5097−5109

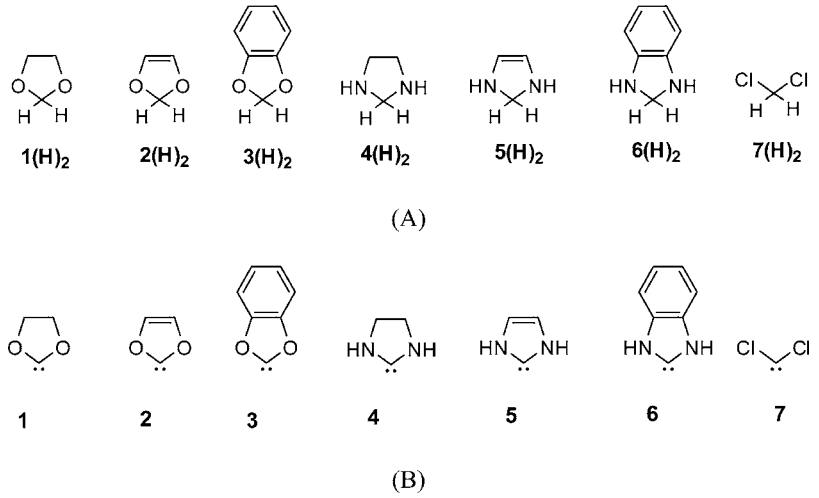

Figure 3. Structures of the (A) proposed substrates denoted as $\mathbf{1(H)_2}$–$\mathbf{6(H)_2}$ and (B) carbenes (**1**–**6**) utilized for the study.

and *Podophyllum hexandrum* shows antimitotic and antiviral activity; which is also known to show MBI of cytochromes.[20] Recently, isoquinoline alkaloids, bulbocapnine, canadine, and protopine, present in herbal medicines were reported as the mechanism-based inactivators of CYP2C19 via MIC formation.[21]

The mechanistic details for the formation of carbene and MIC leading to MBI are still elusive. A few computational studies have been carried out to describe the formation of MIC of Fe-carbene. Semiempirical methods were utilized to describe the MIC for the safrole-based inhibitors.[22] Automated docking was preformed to describe the interaction between CYP3A4 enzyme and deoxypodophyllotoxin and its metabolite, epipodophyllotoxin.[20]

The reported computational and experimental studies point to both the relevance as well as the limitations of MDP-containing compounds. It is evident that several agents with MDP group are in the early phase of testing; however, MDP unit acts as a perpetrator and a significant risk for drug safety due to potential adverse reactions and MBI. Developing effective screening methods for analyzing MBI of cytochromes is in process.[21] Several groups of scientists are involved in the synthesis of compounds containing MDP moiety with the ultimate goal of medicinal applications.[29] It is worth focusing these efforts more toward the metabolically safe compounds with MDP unit; this can be achieved when the mechanistic details associated with RM formation due to MDP moiety become available.

Several plausible reaction schemes for the formation of MDP-carbenes have been proposed.[10−12,25−27] The hypothesized common mechanism involves the formation of the hydroxylated intermediate (I) as shown in Figure 1. Though the first step of the proposed reaction sequence appears to be quite possible, the elimination of water from this intermediate (−CHOH) appears to be unlikely. This leads to doubts regarding the acceptability of this proposed mechanism.

The purpose of this quantum chemical study is (i) to investigate the nature and stability of the MDP-carbene species, (ii) to compare the electronic structure of MDP-carbenes with dichloromethylene (CCl_2) and N-heterocyclic carbenes (NHCs), (iii) to explore the characteristics of MIC of MDP-carbene and heme-iron, (iv) to verify whether the proposed mechanistic pathway (Figure 1) is realistic on the potential energy surface, and (v) to consider the alternative pathways for the formation of MDP-carbene and MIC with heme-iron. Understanding of the structural and energetic details involved in the generation of reactive MDP-carbene can provide several clues regarding the actual biotransformation process of MDP containing compounds. This critical and elaborate theoretical analysis would aid computational, medicinal, and metabolism scientists to consider the perpetrator (MDP moiety) at the early stages of drug discovery and development, and to design leads, which can avoid MBI of CYPs.

COMPUTATIONAL METHODOLOGY

DFT (density functional theory) was utilized to determine the properties of MDP-carbenes and elucidate the reaction pathway leading to the generation of MDP-carbene.[30] Gaussian03 suite of programs was used to carry out all the geometry optimizations and estimate the absolute energies.[31] The B3LYP functional with 6-31+G(d) basis set was used for all geometry optimizations of carbenes.[32] This method has been reported to provide reasonable estimates regarding the characteristics of carbenes.[33,34] For CYP related studies, the B3LYP hybrid density functional was used with LanL2DZ basis set on iron, and the 6-31+G(d) basis set for all remaining atoms.[35] This basis set was designated as **BS1**. A factor of 0.9806 was used to scale zero-point vibrational energies, and values were used for the estimation of absolute energies of all species.[36] The energies were also estimated by single point calculations using the TZVP triple-ζ basis set[37] for iron and 6-311+G(d) basis set for all remaining atoms, designated as **BS2**. Integral equation formalism variant of polarizable continuum model (IEFPCM) was utilized to mimic the protein environment and take into account the bulk polarity effects (denoted as **BS3**) using a nonpolar solvent (chlorobenzene), with a dielectric constant of 5.7.[38] A simple model of iron (IV-oxo) radical cation with heme-porphine and cysteine, SH^-, as the axial ligand (**Cpd I**) to mimic the active site of CYP was used in the study.[28,39] This model has been reported in previous studies, of CYP biotransformation mechanisms, to be sufficiently effective to provide reasonably accurate energy estimates.[40] The reactant and the product complex geometries were optimized to ground state minimum. The transition state geometries on all the reaction pathways were optimized to a first order saddle point and verified to have one imaginary frequency vibrational mode. The reaction profile was explored on both the doublet and quartet spin states of **Cpd I**. Mulliken population analysis was utilized to determine the spin densities, and charge distribution was carried out using NBO method.[41]

dx.doi.org/10.1021/ic400010d | Inorg. Chem. 2013, 52, 5097−5109

Table 1. Singlet-Triplet Energy Difference ($\Delta E_{S\text{-}T}$), Isodesmic Reaction Energies (ΔE_I's), Gibbs Free Energy of Dimerization ($E_{Gibbs\text{-}Dim}$), Energy due to Proton Affinities (PA), and Complexation Energies with BH_3 (E_{BH_3}) in kcal mol^{-1} for the Studied Carbenes

compd no.	name of carbene	$\Delta E_{S\text{-}T}$	ΔE_I	$E_{Gibbs\text{-}Dim}$	first PA	E_{BH_3}
1	dioxocarbene	69.85	83.92	−23.13	219.01	−41.25
2	unsaturated dioxocarbene	74.03	87.83	−16.01	212.22	−40.28
3	MDP carbene	69.59	81.33	−27.75	219.27	−41.61
4	diaminocarbene	72.22	94.18	−14.17	244.90	−50.34
5	NHC	83.20	108.12	4.81	242.96	−49.09
6	benzdiaminocarbene	77.66	102.91	−25.45	244.04	−49.40
7	dichloromethyl carbene	17.73	45.02	−109.94	197.83	−44.83
8	::$C(NHC_H)_2$				282.06	−55.25

RESULTS AND DISCUSSION

This present work reports the characteristics of MDP-carbenes and the elucidation of the actual reaction pathway leading to the generation of this reactive intermediate. Carbenes can be classified into two varieties: reactive and stable carbenes. The stable carbenes are known to show nucleophilicity and form coordination complexes with transition metals.[42] The MDP-carbenes form MIC with heme-iron. Hence, it is intriguing to understand the stability and nucleophilicity of MDP-carbenes in comparison to known stable carbenes like N-heterocyclic carbenes (NHC).[3,42,43] In this Article, the results are presented in three sections: (i) stability and nucleophilicity of MDP-carbenes and comparison with other carbenes, (ii) characteristics and electronic structure of MIC of MDP-carbene and heme iron, and (iii) plausible reaction pathways for the generation of MDP-carbenes.

Electronic Structure and Reactivity of MDP-Carbene. Several carbenes having structural similarity to MDP-carbenes were studied as shown in Figure 3. Many such studies on the electronic structure of carbenes are available in the literature;[33,34,42,43] however, these studies did not include MDP carbenes implicitly. The study by Hollockzi et al. included **1** and **2**, while considering the organocatalytic activity of NHCs.[34e] Various carbenes were generated via the isosteric replacement of oxygen atom with nitrogen, such as diaminocarbenes and N-heterocyclic carbenes (NHCs). The stability of these carbenes was assessed in terms of their singlet−triplet energy difference, isodesmic reaction with methane, and dimerization energy. The nucleophilicity of carbenes was explored in terms of their protonation affinities, complexation with Lewis acids like BH_3. Table 1 lists the quantitative estimates of above-mentioned properties of MDP-carbene **3** in comparison to other carbenes (**1**, **2**, **4**−**7**).

Singlet−triplet energy difference $E_{S\text{-}T}$[43] was estimated by calculating the difference of the zero point corrected energies of the singlet and the triplet species of the carbenes. $E_{S\text{-}T}$ for **1** has been estimated to be 69.85 kcal/mol. $\Delta E_{S\text{-}T}$ for the corresponding unsaturated system **2** is 74.03 kcal/mol. The fusion of phenyl ring with **2** gives **3**, wherein the $\Delta E_{S\text{-}T}$ value gets reduced to 69.59 kcal/mol. These values are much larger than the $\Delta E_{S\text{-}T}$ value for the reactive CCl_2 carbene (17.73 kcal/mol), and comparable to the $\Delta E_{S\text{-}T}$ values of **4**−**6** NHCs (72.22, 83.20, and 77.66 kcal/mol, respectively) indicating that **1**−**3** are highly stable carbenes. The marginally smaller $\Delta E_{S\text{-}T}$ values for **1**−**3** in comparison to **4**−**6** may be attributed to lone pair−lone pair repulsion (between methylene carbon and oxygen atoms of the ring) in **1**−**3**.

The stabilization energies ΔE_I of carbenes can be estimated in terms of isodesmic equations (eq 1).[43f]

$$\text{carbene} + CH_4 \rightarrow :CH_2 + \text{corresponding alkane} \quad (1)$$

The stable NHC carbenes tend to have high ΔE_I values.[33d] The ΔE_I estimated for **1** is 83.92 kcal/mol. This value is increased to 87.83 kcal/mol in the corresponding unsaturated system **2** and decreases to 81.33 kcal/mol in the corresponding benzfused system **3**. Holloczki et al. reported similar values for **1** (84.7 kcal/mol) and **2** (88.2 kcal/mol).[34e] The ΔE_I in CCl_2 carbenes is estimated to be 45.02 kcal/mol, indicating their highly reactive and lesser stable nature. In comparison to the NHCs **4**−**6** (94−108 kcal/mol), the ΔE_I values for **1**−**3** carbenes are lower; therefore, **1**−**3** appear to be moderately stable.

The Gibbs free energy of dimerization (eq 2) provides a more realistic measure of stability of carbenes.[33c]

$$R_2C + R_2C \rightarrow R_2C{=}CR_2 \quad (2)$$

Stable NHC carbenes generally are characterized by low dimerization energies (> −50 kcal/mol), as in **5** (4.81 kcal/mol), and reactive carbenes are characterized by very large dimerization energies (≪ −50 kcal/mol), such as in the case of **7** (−109.94 kcal/mol). The Gibbs free energy of dimerization for **1**, **2**, and **3** are −23.13, −16.01, and −27.75 kcal/mol, respectively. These values clearly indicate that carbenes **1**−**3** are moderately stable and support the data obtained through isodesmic reaction analyses.

It has been proposed that the formation of MIC of carbenes with heme-iron occurs owing to the nucleophilic nature of MDP carbenes.[10,11,13,16] The nucleophilicity criteria for carbenes can be established on the basis of proton affinity energies, and energy for complexation with BH_3.[33,34,42] Absolute proton affinity (APA) of a molecule (B) is calculated using eq 3.[44]

$$\text{APA} = -\Delta H_{298} = H_{298}(B) + H_{298}(H^+) - H_{298}(BH^+) \quad (3)$$

$-\Delta H_{298}$ is the negative of enthalpy change, which includes changes in total energy, zero-point energy (ZPE), vibrational energy while going from 0 to 298.15 K, and rotational and translational energy, as well as a work term (RT = 0.592 kcal/mol). For H^+, the translational energy term is not equal to zero (H_{298} H^+ = 3/2RT = 0.899 kcal/mol at 298.15 K), and a work term is represented as RT = 0.592 kcal/mol.[44] It was observed that the first proton affinity energy for **1**−**3** (212−220 kcal/mol) was lower than that for **4**−**6** (242−245 kcal/mol). Holloczki et al. reported similar pattern for the proton affinities for a variety of carbenes, possessing nitrogen, oxygen, and sulfur atoms in the order N > S > O.[34e] The energy due to

dx.doi.org/10.1021/ic400010d | Inorg. Chem. 2013, 52, 5097−5109

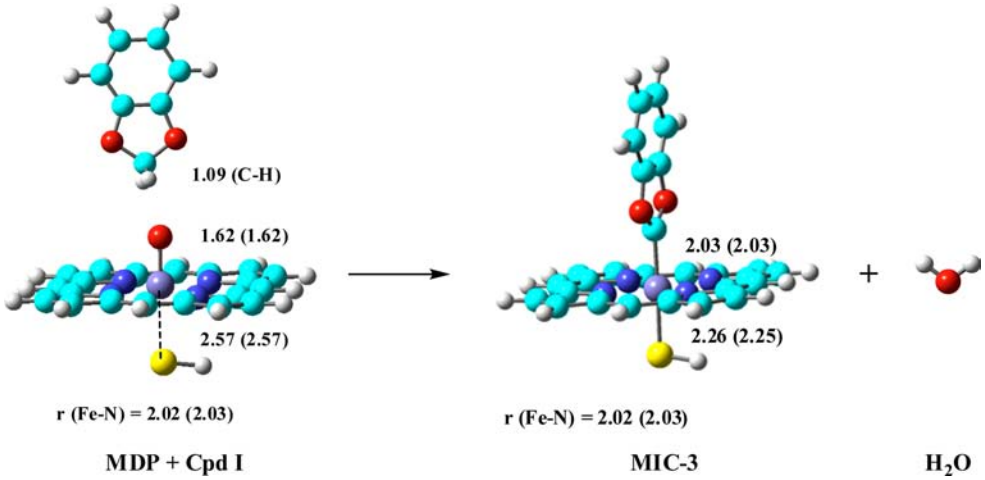

Figure 4. BS3-optimized geometries of the reactants, methylenedioxyphenyl, MDP moiety; **Cpd I**; and **MIC-3**: MIC of MDP-carbene and heme-iron. The values are shown for doublet and (quartet) spin states of **Cpd I**. All the bond distances are in Å and bond angles in degrees (°). The average distance of Fe−N bonds in heme-porphine is also shown for each species. Color code: red, oxygen; sky blue, carbon; white, hydrogen; blue, nitrogen; gray, iron; yellow, sulfur.

complexation with BH_3 is the difference between the energies of carbene-BH_3 complex and the energies of the isolated carbene and BH_3 molecule.[33,34,42] The energies due to complexation of **1**−**3** with BH_3 (−40 to −42 kcal/mol) were found to be lower than that of NHCs **4**−**6** (−49 to −51 kcal/mol), similar to the proton affinity energies. The energy of −41.61 kcal/mol for MDP-carbenes provides an indication of it being sufficiently nucleophilic. All the parameters listed in Table 1 establish that the MDP-carbenes are moderately stable and reasonably nucleophilic. Carbenes **3** and **6** are quite similar in terms of π delocalization. Carbene **3** is clearly less stable and nucleophilic than **6**, presumably because of lone pair (O)−lone pair (C) repulsion in **3** and greater electronegativity of O

Characteristics and Electronic Structure of MIC. The MIC of MDP-carbene and heme-iron, **MIC-3** (Figure 4), was observed to be highly stable. The reaction leading to the formation of **MIC-3** (equation in Figure 4) is exothermic by −40.35 kcal/mol using **BS3** basis set, under solvent (ε = 5.7) conditions (IEFPCM).

Table 2 shows the energies (at **BS1** and **BS3** basis sets) for the formation of MIC for all the studied carbenes. The carbene-iron coordination (C:···Fe) distances for the respective MICs are also shown. **MIC-1** and **MIC-2** are stable with the energies of −44.97 and −47.34 kcal/mol, respectively. MIC for NHCs **4**−**6** are highly stable with energies ranging from −61 to −76 kcal/mol.

Table 2. Energies for the MIC (in kcal/mol) and Iron-Carbene Distance (in Å) for the Iinvestigated Carbenes Calculated at BS1 and BS3 Basis Set

		ΔE_{MIC} (kcal/mol)		
carbene	MIC	BS1	BS3	Fe···:C distance (Å)
1	**MIC-1**	−37.96	−44.97	2.04
2	**MIC-2**	−40.92	−47.34	2.04
3	**MIC-3**	−33.28	−40.35	2.03
4	**MIC-4**	−58.86	−61.60	2.04
5	**MIC-5**	−72.78	−76.27	2.03
6	**MIC-6**	−65.57	−68.22	2.04

A significant difference in the stability of **MIC-3** on the doublet (−40.35 kcal/mol) and quartet (−5.91 kcal/mol) spin states of **Cpd I** was observed. The MIC formed on the quartet spin surface was observed to be less stable, owing to the excitation observed from the carbene center where, the singlet−triplet carbene transition occurred within the carbene unit, rather than excitation within the metal d-orbitals. The vibrational analysis of **MIC-3** using DFT calculation indicates a significant vibrational frequency (C−O stretching: 1229.39 cm^{-1}) for the interaction between **3** and heme-iron (see Supporting Information, Figure S5). The experimentally reported C−O stretching frequencies lie in the range 1000−1300 cm^{-1}, while the corresponding C−O stretching frequency in the isolated MDP carbene was lower (1128.65 cm^{-1}), indicating a significant influence of the proximity to heme-iron in **MIC-3**. In **MIC-3**, the C:···Fe coordination bond distance was observed to be 2.03 Å, indicating a strong coordination complex. It is interesting to note that the Fe−S distance is reduced from 2.57 to 2.26 Å in **MIC-3**. Also, the Fe−C−O plane is perpendicular to that of Fe−SH plane in **MIC-3**. These facts indicate that Fe−C and Fe−S bonds are stabilized by the orthogonal iron d-orbitals and the balance in the σ- and d-orbital interaction between MDP carbene and Fe is readjusted upon bonding with the carbene.

Molecular orbital analysis was carried out for **3**, **5**, heme-iron-porphyrin, **MIC-3**, and **MIC-5**. The HOMO and LUMO of **3**, **5**, and heme-iron-porphyrin were observed to identify the orbitals participating in complexation. Thereafter, the orbitals of **MIC-3** and **MIC-5** were analyzed. On the basis of the interacting orbitals and respective energies in eV, the orbital interaction diagram of Figure 5 was drawn. Figure 5 (left-hand side) shows the orbital interaction diagram for the donor−acceptor interactions between **3** and heme-porphine, giving rise to **MIC-3**. From the interaction diagram, it can be clearly seen that the σ lone pair of MDP carbene is involved in σ bonding with the empty d_{z^2} orbital of iron center. The a_{2u} of heme-porphine is observed to stabilize this σ bonding. The interaction of a_{2u} orbital with σ orbital of carbene leads to higher energy (−4.98 eV) HOMO (singly occupied). The filled d_{xz} orbital of heme-iron is involved in π back-bonding interaction (−7.98 eV) with the unoccupied p orbital of

dx.doi.org/10.1021/ic400010d | Inorg. Chem. 2013, 52, 5097−5109

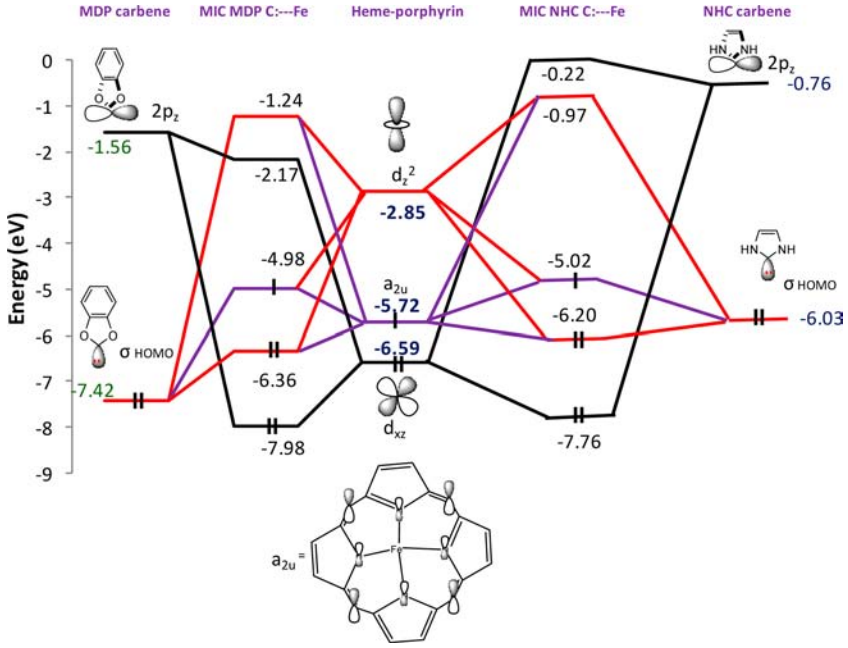

Figure 5. Orbital interaction diagram for interactions between MDP carbene and heme-porphine leading to **MIC-3** (on left-hand side), and interactions between NHC and heme-porphine leading to **MIC-5** (on right-hand side). The ordering of the orbitals follows the calculated eigenvalues in electron volts (eV). Dotted red line indicates orbital interaction between σ and d_{z^2}, dotted purple line indicates orbital interaction between σ and a_{2u}, and dotted black line indicates π back-bonding interaction between d_{xz} and empty p orbital.

Scheme 1. Proposed Reaction Pathway-I with Mechanistic Details for the Generation of Reactive Carbene Intermediate, and Formation of MIC with Heme-Iron[a]

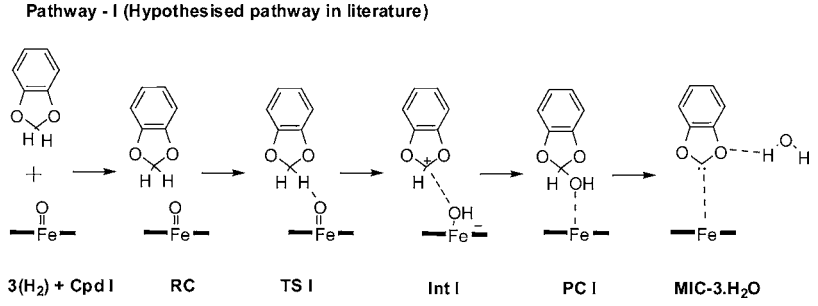

[a]**RC**, reactant complex of MDP [**3**(H_2)] and **Cpd I**; **TS I**, transition state for H-abstraction by **Cpd I**; **Int I**, intermediate; **PC I**, product complex of hydroxylated product and heme-porphine; **PC II**, product complex of **MDP**-carbene (**3**); water and heme-porphine, **MIC-3·H_2O**. The bold lines along with Fe represent the heme-porphine group, with SH^- as the axial ligand.

carbene. The interactions were found to be similar for both α and β spin components of the iron-porphyrin. The second order interaction energy, $E^{(2)}$, for the coordination of MDP carbene to heme-iron was estimated to be 51.0 kcal/mol. The mixing between σ_{LP} of carbene and d_{z^2} of heme-iron was observed to be strong, as evident by 49.06% p-contribution and 39.11% d-contribution (NBO analysis). $E^{(2)}$ for π back-bonding interaction was estimated to be 3.70 kcal/mol in the stabilization of **MIC-3**. The back-bonding contribution has been reported to be dependent on the metal, ancillary ligands, and the geometric environment.[3c] The back-bonding contribution for various NHCs has been reported to be ranging from 5 to 20 kcal/mol.[3c] All these interactions (σ donation and π back-donation) are contributing to the Fe−:C coordination and providing stability to **MIC-3**.

On the right-hand side of Figure 5, the orbital interaction diagram of NHC (**5**) and heme-porphine leading to the highly stable **MIC-5** is shown. The energy of the LUMO of MDP carbene **3** is considerably lower than that of NHC **5**. Therefore, a marginally stronger π interaction is seen in **MIC-3** than in the corresponding **MIC-5**. The energy gap in **MIC-5** between the bonding and antibonding molecular orbitals for iron-d_{xz}-π*carbene interaction is higher (7.54 eV) than in **MIC-3** (5.81 eV). The energy gap between the bonding and antibonding molecular orbitals for σ_{LP} carbene and d_{z^2} heme-iron is nearly similar in both the complexes, **MIC-3** (5.06 eV) and **MIC-5** (5.23 eV). Thus, the above orbital analysis implies the formation of stable MIC for both MDP carbenes and NHCs (Table 2).

This orbital analysis supports the reported experimental studies that the MDP containing compounds are quasi-irreversible inhibitors of CYPs implying that the inhibition can be reversed under suitable conditions. Thus, the drug−drug interactions occurring due to CYP inhibition by the MDP carbene-iron coordination have been reported in a few cases.[11−23] On the other hand, the NHCs-based carbene-iron

dx.doi.org/10.1021/ic400010d | Inorg. Chem. 2013, 52, 5097−5109

complexes (MIC **4**–**6**, Table 2) are quite strong, and may prove to be extremely toxic and perilous.

Elucidation of Reaction Pathways for the Generation of MDP-Carbenes. After understanding the electronic structure of MDP-carbene and that of **MIC-3**, the reaction pathway for the generation of carbene and MIC formation was explored using density functional theory. Initially, the pathway proposed in literature (**Pathway-I**) was studied in detail to account for its feasibility in the generation of MIC with heme-iron. MDP denoted as $[\mathbf{3(H)_2}]$ was used as the model substrate and **Cpd I** as the model oxidant for the study. The results are reported using the basis set **BS3**, taking into account bulk polarity effects and zero point corrections, unless otherwise specified.

Pathway-I: CH Hydroxylation Followed by Water Elimination. The **Pathway-I** for the formation of MDP-carbene is shown in Scheme 1. **Pathway-I** involves the initial step of hydrogen abstraction by **Cpd I**, which is a known reaction for a variety of substrates in heme and nonheme enzymes.[39,40,45] The hydrogen abstraction from the methylene carbon of $\mathbf{3(H)_2}$ generates substrate radical, $\mathbf{3(H)^{\bullet}}$, and **Cpd I**-H via homolytic cleavage. On the other hand, heterolytic cleavage of $\mathbf{3(H)_2}$ results in the formation of $\mathbf{3(H)^+}$ and **Cpd I**-H^-.

Quantitative estimation of enthalpies for homolytic and heterolytic cleavage of all the proposed substrates (Figure 3) of model carbenes was carried out and compared with that of methane molecule (Table 3). A comparison between hydrogen

Table 3. Comparative Analysis of the Homolytic and Heterolytic Cleavage of Methane and Studied Substrates, $\mathbf{1(H)_2}$–$\mathbf{6(H)_2}$, Using Cpd I (Doublet Spin State) as the Model Oxidant[a]

S no.	reaction	enthalpy (kcal/mol)
	Homolytic Cleavage	
1	CH_4 + **Cpd I** → $CH_3^{\bullet}$ + **Cpd I**–H	30.51
2	$\mathbf{1(H)_2}$ + **Cpd I** → $\mathbf{1(H)^{\bullet}}$ + **Cpd I**–H	21.99
3	$\mathbf{2(H)_2}$ + **Cpd I** → $\mathbf{2(H)^{\bullet}}$ + **Cpd I**–H	20.19
4	$\mathbf{3(H)_2}$ + **Cpd I** → $\mathbf{3(H)^{\bullet}}$ + **Cpd I**–H	22.17
5	$\mathbf{4(H)_2}$ + **Cpd I** → $\mathbf{4(H)^{\bullet}}$ + **Cpd I**–H	15.99
6	$\mathbf{5(H)_2}$ + **Cpd I** → $\mathbf{5(H)^{\bullet}}$ + **Cpd I**–H	−2.06
7	$\mathbf{6(H)_2}$ + **Cpd I** → $\mathbf{6(H)^{\bullet}}$ + **Cpd I**–H	7.56
	Heterolytic Cleavage	
8	CH_4 + **Cpd I** → CH_3^+ + **Cpd I**–H^-	87.25
9	$\mathbf{1(H)_2}$ + **Cpd I** → $\mathbf{1(H)^+}$ + **Cpd I**–H^-	−7.19
10	$\mathbf{2(H)_2}$ + **Cpd I** → $\mathbf{2(H)^+}$ + **Cpd I**–H^-	−5.89
11	$\mathbf{3(H)_2}$ + **Cpd I** → $\mathbf{3(H)^+}$ + **Cpd I**–H^-	0.23
12	$\mathbf{4(H)_2}$ + **Cpd I** → $\mathbf{4(H)^+}$ + **Cpd I**–H^-	−42.94
13	$\mathbf{5(H)_2}$ + **Cpd I** → $\mathbf{5(H)^+}$ + **Cpd I**–H^-	−65.33
14	$\mathbf{6(H)_2}$ + **Cpd I** → $\mathbf{6(H)^+}$ + **Cpd I**–H^-	−47.93

[a]The relative energies, in kcal/mol, are calculated at **BS3** basis set.

abstraction data versus hydride ion abstraction data in Table 3 clearly indicates that $\mathbf{1(H)_2}$–$\mathbf{6(H)_2}$ prefer to follow a heterolytic cleavage pathway. Table 3 shows that, in $\mathbf{3(H)_2}$, heterolytic cleavage involving hydride ion transfer (0.23 kcal/mol) is much more favorable than the homolytic cleavage involving hydrogen radical transfer (22.17 kcal/mol). In comparison, heterolytic cleavage for methane is highly improbable, owing to a highly endothermic reaction (87.25 kcal/mol).

Figure 6 shows the 3D structures of the reactant complex (**RC**), intermediate (**Int I**), transition state (**TS I**), and product complex (**PC I**) on both the doublet and quartet spin states involved in **Pathway-I**. The discussion for **Pathway- I** is with respect to the more favorable doublet spin state of **Cpd I**. **Cpd I** and $\mathbf{3(H)_2}$ initially form a reactant complex, **RC**, where the methylene hydrogen atom of MDP shows an interaction (2.23 Å) with the oxo group (O═Fe) of **Cpd I**. The Fe═O distance is observed to be 1.62 Å, and the Fe–O–H bond angle was observed to be 157.8°. The reactant complex **RC** is slightly less stable by 0.55 kcal/mol than the isolated reactants, $\mathbf{3(H)_2}$ and **Cpd I**, as shown in the energy profile (Figure 7). The rate determining step on **Pathway-I** is observed to be the hydride ion transfer (Figure 7), with an activation barrier of 8.92 kcal/mol, via transition state **TS I**. The Fe═O bond length increases to 1.70 Å in **TS I** from 1.62 Å in **RC**. The methylene hydrogen (C–H) approaches the oxo group, facilitating the H-abstraction process, as observed by the decrease in bond distance (H–O) from 2.23 to 1.34 Å. Also, in **TS I**, a colinear arrangement of O–H–C can be clearly observed. Thus, the lower activation barriers (<9 kcal/mol) on the doublet spin state of **Cpd I** suggests that the hydride ion transfer reaction is facile for this substrate.

The hydride ion transfer results in the formation of intermediate **Int I**, slightly endothermic by 0.50 kcal/mol. **Int I** is found to be much more stable than the corresponding isolated species, i.e., $\mathbf{3(H)^{\bullet}}$ and **CpdI**-H by −21.67 kcal/mol. This high stability prompted us to study the possibility of heterolytic cleavage (Table 3) in $\mathbf{3(H)_2}$, and **Int I** was observed to be a complex of $\mathbf{3(H)^+}$ and **CpdI**-H^-. Similar hydride ion transfer mechanism by iron(IV)-oxo porphyrin has been reported for several dihydronicotinamide adenine dinucleotide (NADH) analogues, 10-methyl-9,10-dihydroacridine ($AcrH_2$), 1-benzyl-1,4-dihydronicotinamide (BNAH), etc.[46]

In **Int I**, C–H distance is significantly elongated (2.15 Å), and a significant increase in spin density on oxygen atom (0.23) attached to heme-iron in **Int I** is observed, as compared to 0.07 in the transition state. This also supports the $\mathbf{3(H)^+}$ and **CpdI**-H^- character of **Int I**. In the next step of the reaction, **Int I** directly leads to the formation of a stable hydroxylated product, **PC I** (Figure 7) on the doublet spin state through a barrierless rebound process. The C–O bond distance is observed to be 1.41 Å in **PC I**, indicating the formation of the hydroxylated product. The increase in Fe–O distance in **PC I** (2.37 Å) as compared to **Int I** (1.78 Å) implies that the transfer of electron density from Fe–O bond to C–O bond, leading to the formation of hydroxylated product. Similar results have been reported for CH-hydroxylation in methane and propane.[47] **PC I** is observed to be stable by −57.12 kcal/mol on an exothermic reaction. The next step leading to the carbene generation is endothermic by 16.76 kcal/mol on the doublet spin state of **Cpd I**. It is not clear how and why highly stable **PC I** shall be involved in an endothermic reaction. The direct water elimination from **PC I** to yield **MIC-3·H_2O** was studied; however, all attempts to trace this water elimination step using quantum chemical methods failed.

Therefore, **Pathway-I** does not seem to be the acceptable pathway for the formation of MIC complex from MDP, owing to the very high stability of **PC I** and its unlikely conversion to a less stable carbene intermediate. As a consequence, **Pathway-I** cannot be considered as the possible option leading to the MDP-carbene formation.

Since the pathway reported in literature seems unrealistic, it becomes fundamentally interesting to explore the alternative pathways. To the best of our knowledge, no alternative

dx.doi.org/10.1021/ic400010d | Inorg. Chem. 2013, 52, 5097–5109

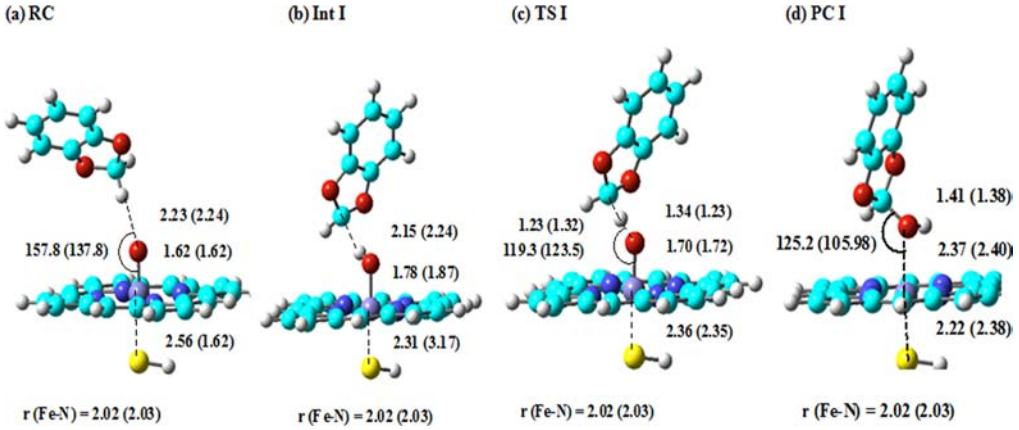

Figure 6. BS3-optimized geometries of the key species involved in **Pathway-I**. The values are shown for doublet spin state of **Cpd I**. All the bond distances are in Å and bond angles in degrees (°). The average distance of Fe−N bond distances in heme-porphine is also shown for each species. Data on the quartet spin state of **Cpd I** is given in Supporting Information (Figure S2). Color code: red, oxygen; sky blue, carbon; white, hydrogen; blue, nitrogen; gray, iron; yellow, sulfur.

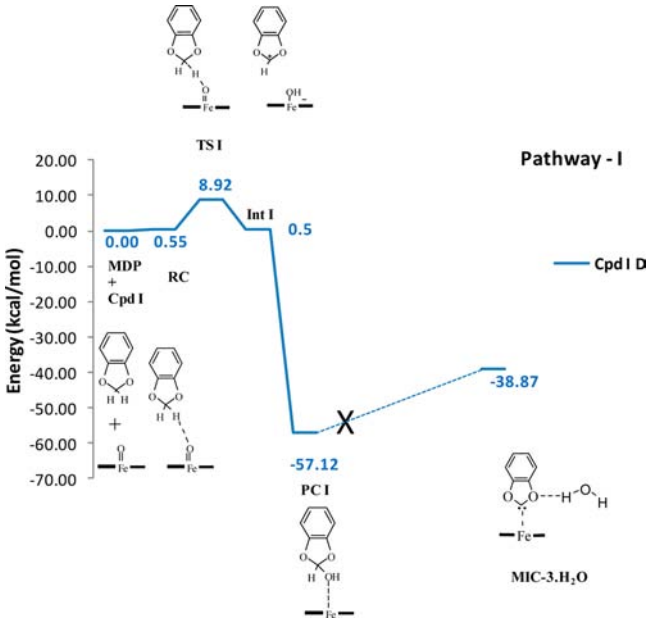

Figure 7. Potential energy surface for the reaction **Pathway-I** on the doublet (D) spin surface of **Cpd I** at **BS3** basis set. The energies are in kcal/mol relative to the isolated reactants. The cross X indicates the unfavorable reaction pathway for the formation of carbene. The potential energy surface on the quartet spin state of **Cpd I** is given in the Supporting Information (Figure S2).

pathways have been proposed or studied in literature or experimental studies.[11,23−26] Three alternative pathways have been proposed as shown in Scheme 2: (i) **Pathway-II**, hydride ion abstraction followed by proton transfer and subsequent water elimination; (ii) **Pathway-III**, proton shuttle pathway via porphyrin nitrogen followed by water elimination; and (iii) **Pathway-IV**, direct generation of carbene via simultaneous abstraction of two methylene hydrogen atoms, one H-abstraction by Fe═O and the other by the nitrogen atom of porphyrin as in proton shuttle pathway, followed by water elimination.

Pathway-II. Figure 8 (right-hand side) shows the energy profile for this pathway on the doublet spin state of **Cpd I**. It can be observed that the first step of **Pathway-II** remains similar to that of **Pathway-I**; however, the intermediate **Int I** leads to the generation of a more stable intermediate (**Int II**) as shown in Figure 9. The major difference between **Int I** and **Int II** is the $C^{+}\cdots H-O(Fe)^{-}$ in **Int I** versus the $C^{+}-H\cdots O-(H)(Fe)^{-}$ interaction in **Int II**.

In this transformation, instead of C···O interaction, a C−H···O interaction predominates the reaction. All the attempts to locate a transition state between **Int I** and **Int II** did not yield any viable transition state structure; thus, the generation of $\mathbf{3(H)^{+}}$ leading to the formation of **Int II** is a spontaneous and exothermic reaction with the product enthalpy of −20.46 kcal/mol on the doublet spin state. **Int II** can be treated as an intermediate during rebound of $\mathbf{3(H)^{+}}$, where the H-atom of $\mathbf{3(H)^{+}}$ is directly involved in the rebound process. **Int II** can directly lead to the formation of MDP-carbene (**PC II**) via a transition state involving proton transfer (negative imaginary frequency, 539.13 cm^{-1}), requiring a very small activation barrier of 0.12 kcal/mol (nearly a barrierless step) on the doublet spin surface (Figure 8). **PC II** (Figure 9) comprises **3** and water bound to heme-porphine, where the carbene shows the interaction of its lone pair with the H-atom of water bound to heme-iron.

The increase in Fe−O distance (2.14 Å, doublet) in **PC II** implies that the water molecule formed via **TS II** can be easily displaced by the MDP-carbene (**3**), resulting in the formation of **MIC-3·H_2O**, where a coordinate bond interaction between the MDP-carbene and heme-iron is observed. The transition state for the displacement of water molecule attached to heme-iron by **3** was elucidated (**TS-we** in Figure 9). The energy barrier for this reaction was observed to be 11.69 kcal/mol on the doublet spin state of **Cpd I**. It can be observed that the C:···Fe and Fe···H(OH) bond distances are nearly similar (3.36 and 3.38 Å) indicating the feasibility of this transition state and displacement of the water molecule attached to heme-iron by the MDP-carbene. The complex, similar to **PC II**, has been reported for the binding of azole inhibitors in the active site of cytochrome.[48] Balding et al. reported the approach of azole inhibitor toward heme,[48] and later displacement of water molecule from the heme by the inhibitor, as observed in our study (**MIC-3·H_2O**). The **MIC-3·H_2O** shows the MDP-carbene bound to heme-iron, with a hydrogen bonding interaction with the water molecule in the active site cavity of cytochrome. This displacement of water molecule by **3** actually blocks the dioxygen binding, resulting in the inactivation of

dx.doi.org/10.1021/ic400010d | *Inorg. Chem.* 2013, 52, 5097−5109

Scheme 2. Proposed Reaction Pathways- II, -III, and -IV with the Mechanistic Details for the Generation of Reactive Carbene Intermediate, and Formation of MIC with Heme-Iron[a]

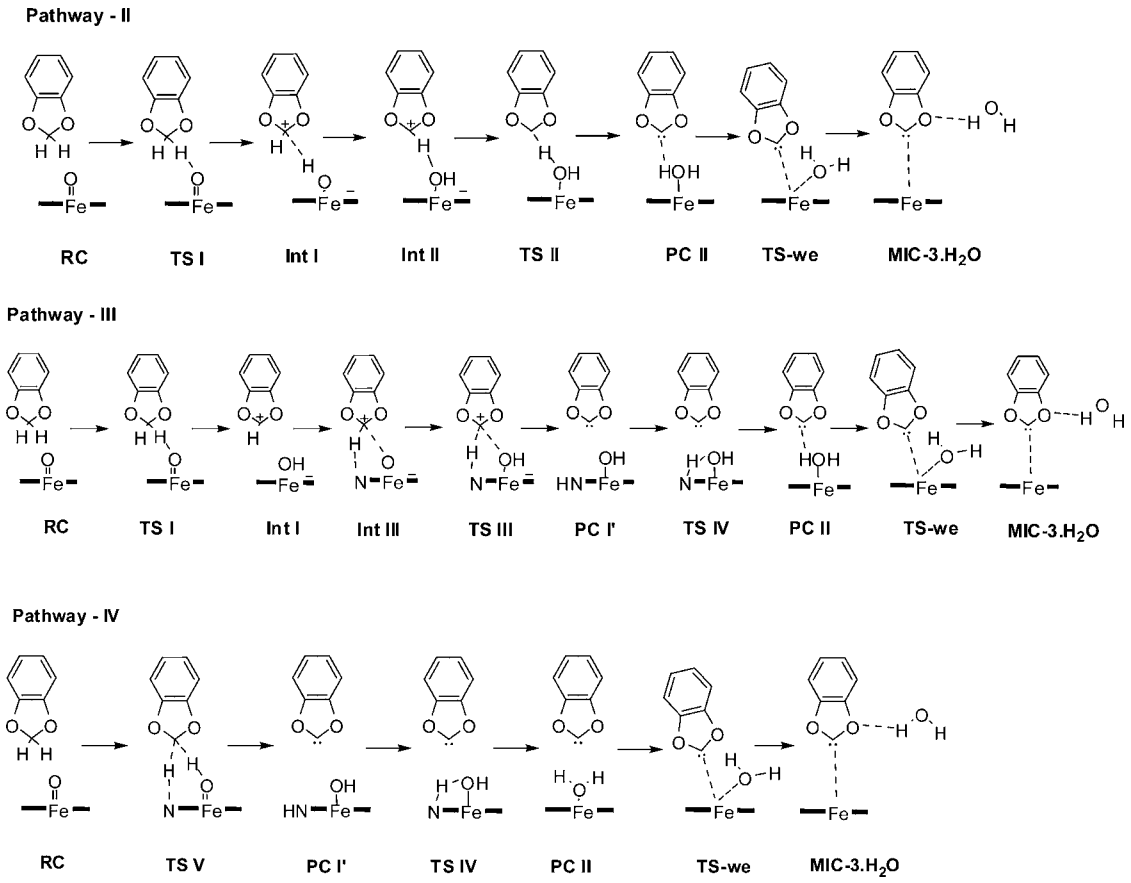

[a]The bold lines along with Fe represent the heme-porphine group, with SH^- as the axial ligand. N refers to the heme-porphyrin nitrogen.

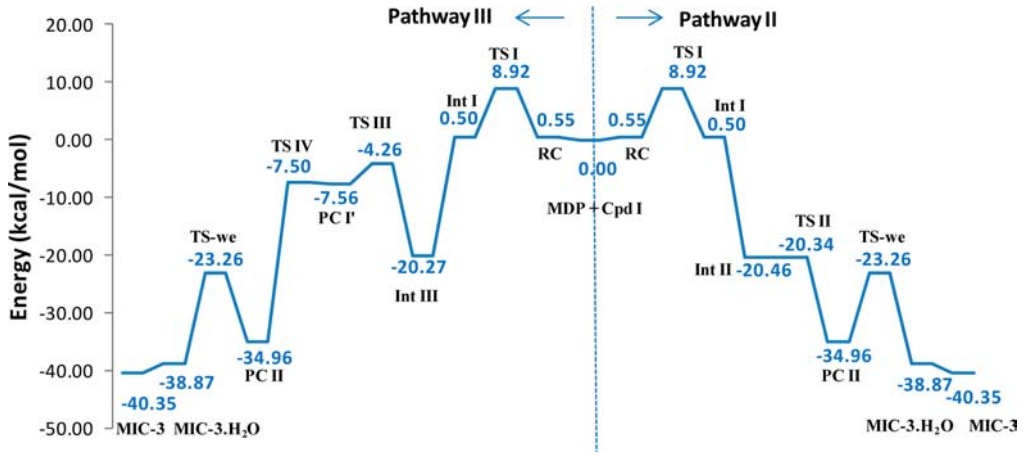

Figure 8. Potential energy surface for the reaction **Pathway-II** and **-III** on the doublet spin surface of **Cpd I** at **BS3** basis set. The energies are in kcal/mol relative to the isolated reactants, MDP and **Cpd I**.

heme center. The H-bonding interaction in **MIC-3·H_2O** between the oxygen atom of MDP ring and the hydrogen of the eliminated water is weak (2.72 Å, doublet and 2.64 Å, quartet). In **PC II**, the energies of doublet (−34.96) and quartet (−33.01) spin states are very close; however, the reaction occurs preferably on the doublet state, since the MDP-carbene-bound inhibitor complex (**MIC-3**) is the lowest in energy on this spin state.

Pathway-III. Figure 8 (left-hand side) shows the calculated reaction energy profile for **Pathway-III** on the doublet spin state of **Cpd I**. This pathway involves a similar hydride ion transfer step, as discussed in the previous reaction pathway. However, **Int I** may lead to another stable intermediate (**Int III**) with an exothermicity of 20.27 kcal/mol. **Int III** (Figure 9) differs significantly from **Int II**, with respect to the orientation of **3(H)**$^+$, especially the position of the second methylene H-atom. **Int III**, similar to **Int II**, possesses a cationic character on

dx.doi.org/10.1021/ic400010d | Inorg. Chem. 2013, 52, 5097−5109

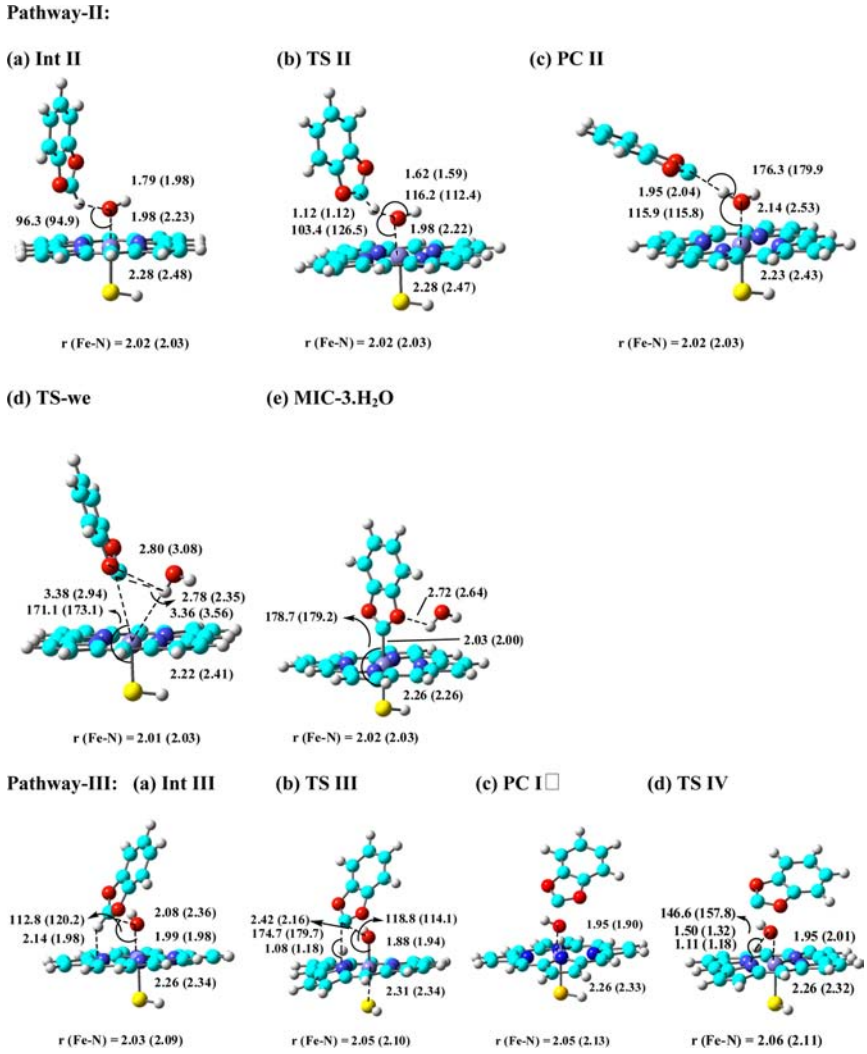

Figure 9. **BS3**-optimized geometries of the key species involved in **Pathway-II** and **-III**. **PC II**, **TS-we**, and **MIC-3·H_2O** are common for all the pathways. The values are shown for doublet and (quartet) spin states of **Cpd I**. All the bond distances are in Å and bond angles in degrees (°). The average distance of Fe−N bond distances in heme-porphine is also shown for each species. Color code: red, oxygen; sky blue, carbon; white, hydrogen; blue, nitrogen; gray, iron; yellow, sulfur.

the substrate, **3(H)**$^+$, upon the electrostatic interaction of methylene hydrogen with the porphine nitrogen. This H-atom shows proximity toward porphyrin nitrogen (2.14 Å, doublet, and 1.98 Å, quartet), and the plane of the MDP ring is perpendicular in orientation to the plane of the heme-porphyrin. Hence, the geometrical features of **Int III** are suitable for proton transfer from **3(H)**$^+$ to the N-atom of porphyrin ring, similar to the reported proton shuttle pathway.[28,49] The transition state geometry for the proton shuttle, **TS III**, is shown in Figure 10. The N−H−C bond angle in **TS III** is observed to be ∼175−180°, favoring the H-abstraction by porphyrin nitrogen (proton shuttle to the porphyrin nitrogen). The H-atom clearly shows transition from carbon of substrate to the porphyrin nitrogen, as observed by the bond distances (N···H: 1.08 Å, doublet). The Fe−O−C bond angle (118.8°) does not show considerable change with respect to **Int III** (112.8° and 120.2°), as shown in Figure 9. This indicates that, indeed, **TS III** is feasible on this reaction pathway. This step requires an energy barrier of 16.02 kcal/mol on the doublet spin state. A significant buckling of the porphyrin ring, due to the protonation of the porphyrin nitrogen, was observed in **TS III**. The pyrrole ring shows a

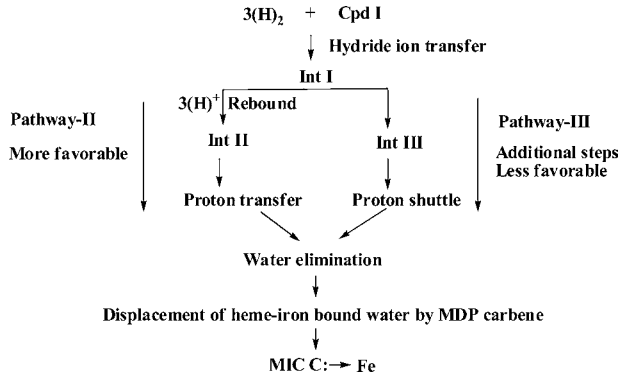

Figure 10. Schematic representation for the preference of **Pathway-II** leading to **MIC-3** in comparison with **Pathway-III**.

deviation of 29.53° from the mean plane of the rest of the porphyrin (Figure 10). A similar buckling was observed by our group in the proton shuttle during the hydroxylation of methylamine, ultimately leading to the generation of nitroso intermediate and MIC formation with heme-iron.[28] Shaik and de Visser have reported a similar buckling in the proton shuttle

dx.doi.org/10.1021/ic400010d | Inorg. Chem. 2013, 52, 5097−5109

mechanism of benzene hydroxylation.[49] Thus, the proton shuttle step can lead to the formation of the MDP-carbene intermediate and heme-porphine with iron-hydroxo group and protonated porphyrin nitrogen (**PC I′**) as shown in Figure 9. Thus, **Pathway-III** involves an endergonic reaction for the formation of **PC I′** (similar to **Pathway-I**). **PC I′** is stable by −7.56 kcal/mol (doublet) and can easily undergo water elimination (**TS IV**) via an almost barrierless reaction (Figure 8). The N−H−O bond angle in **TS IV** is observed to be 146.6° (doublet), indicating the likelihood of proton transfer to oxygen atom attached to heme-iron. The N−H bond distance in **TS IV** is elongated to 1.11 Å, while the H−O bond distance decreases to 1.50 Å on the doublet spin state. This step ultimately leads to the stable MIC of MDP-carbene and heme-iron (**MIC-3**) via the displacement of water molecule by the MDP-carbene (**TS-we**) as discussed for **Pathway-II**.

Pathway-IV. An additional path involving simultaneous activation of both the C−H bonds of $\mathbf{3(H)_2}$ was considered, in which one H atom is transferred to Fe═O center and the other H atom is transferred to N atom of heme-porphine ring. Figure S4 shows the energy profile for this pathway, where the rate determining step involves the simultaneous abstraction of two hydrogen atoms from $\mathbf{3(H)_2}$ by Fe═O and porphyrin nitrogen. This requires a very large activation barrier (∼41 kcal/mol), thus undermining the suitability of this pathway for the formation of MDP-carbene.

Thus, the detailed study of all the reaction pathways emphasized that carbene formation involves a hydride transfer mechanism rather than a hydrogen radical pathway. It can also be inferred by the reaction energy profiles that **Pathway-II** is the most plausible reaction pathway leading to the formation of the MDP-carbene (**3**), and MIC of MDP-carbene with heme-iron (Figure 10). The mechanistic pathway involving proton shuttle to porphyrin ring may be an alternative option in which the overall reaction barrier remains the same as in **Pathway-II**; however, it involves the formation of an endothermic intermediate via a significant energy barrier.

CONCLUSIONS

The drugs containing methylenedioxyphenyl (MDP) group are known to cause mechanism-based inhibition of CYP450, via the formation of carbenes and consequently metabolic-intermediate complex (MIC) with prosthetic heme-iron. A detailed study on a variety of carbenes structurally similar to MDP-carbene was undertaken, and the results were compared with nitrogen analogues (O replaced by N) of the same carbenes. The stability, nucleophilicity, and reactivity of all these carbenes was assessed in terms of several parameters studied using quantum chemical methods. The results indicated that MDP-carbenes are characterized by sufficient stability and reactivity in specific comparison to highly stable N-heterocyclic carbenes and reactive CCl_2 carbenes. It was also observed that MDP-carbenes show comparative nucleophilicity as N-heterocyclic carbenes (NHCs). The stability of the MIC of MDP-carbene and heme-iron was assessed, where the carbene-iron coordination (2.03 Å) was observed to arise from the interaction between σ_{LP} of carbene and empty d_{z^2} orbital of heme-iron, aided by back-bonding interaction between d_{xz} and empty p orbital of carbene. The MIC of MDP-carbene and heme-iron was observed to be highly stable, as indicated by the complexation energy of −40.35 kcal/mol. This binding of MDP-carbene with heme-iron renders the heme center inactive, thus leading to cytochrome inhibition via MIC, which was observed in reported UV spectral studies. The atomistic details of the metabolic reaction pathways leading to the formation of the reactive metabolite, MDP-carbene and MIC, were studied. The basis set **BS3** incorporating solvent effects and zero point corrections was employed to study the reaction between MDP and model oxidant, **Cpd I** (doublet and quartet spin states) to explore the potential energy surface toward the generation of nucleophilic MDP-carbene. The reported pathway (in literature, **Pathway- I**) involving the formation of a hydroxylated product was discarded owing to the high exothermicity and stability (∼57−62 kcal/mol) of this hydroxylated product (−CHOH), and it generates less stable carbene via an unfavorable endothermic reaction. The initial step in the pathway involved a heterolytic cleavage leading to hydride ion transfer (0.23 kcal/mol) as compared to the homolytic cleavage (hydrogen radical transfer, 22.17 kcal/mol). It was also observed that all the substrates, $\mathbf{1(H_2)}$−$\mathbf{6(H_2)}$, studied follow a favorable heterolytic cleavage pathway.

Three alternative pathways were proposed and explored: (i) **Pathway-II**, hydride ion abstraction followed by proton transfer and subsequent water elimination; (ii) **Pathway-III**, proton shuttle via heme-porphyrin ring; (iii) **Pathway-IV**, direct generation of carbene via simultaneous activation of two C−H bonds by **Cpd I** followed by water elimination. **Pathway-II** is the most likely pathway on the whole potential energy surface, owing to the greater stability of intermediates and more favorable activation barriers, as compared to other pathways.

ASSOCIATED CONTENT

Supporting Information

NBO charge and Mulliken spin density analysis for key optimized species (Table S1 and Table S2), absolute energies of the key geometries at **BS2** and **BS3** basis set (Table S3), transition state for rebound mechanism on quartet spin state (Figure S1), reaction energy profile and structures of intermediate and transition state for **Pathway-I** on both the spin states of **Cpd I** (Figure S2), reaction energy profile for **Pathway-II**, **Pathway-III**, and **Pathway-IV** on the quartet spin state of **Cpd I** (Figure S3), potential energy surface for the reaction **Pathway-IV** on the doublet spin surface of **Cpd I** (Figure S4), vibrational analysis (IR spectrum) for C−O stretching in **MIC-3** (Figure S5), and Cartesian coordinates for key optimized species discussed in the text. This material is available free of charge via the Internet at http://pubs.acs.org.

AUTHOR INFORMATION

Corresponding Author

*E-mail: pvbharatam@niper.ac.in. Phone: +91 172 2292018. Fax: +91 172 2214692.

Notes

The authors declare no competing financial interest.

ACKNOWLEDGMENTS

This research was financially supported by the Department of Science and Technology (DST), New Delhi. N.T. thanks the DST for the INSPIRE Fellowship.

REFERENCES

(1) (a) Albrecht, M. *Science* **2009**, *326*, 532−533. (b) Lavallo, V.; Grubbs, R. H. *Science* **2009**, *326*, 559−562. (c) *Reactive Intermediate Chemistry*; Moss, R. A., Platz, M. S., Jones M., Jr., Eds.; Wiley: New York, 2004.

(2) (a) Grasa, G. A.; Kissling, R. M.; Nolan, S. P. *Org. Lett.* **2002**, *4*, 3583−3586. (b) Hedrick, J. L.; Waymouth, R. M.; Connor, E. F.; Lamboy, J. A.; Nyce, G. W.; Connor, E. F. *Org. Lett.* **2002**, *124*, 3587−3590. (c) Neilson, B. M.; Bielawski, C. W. *J. Am. Chem. Soc.* **2012**, *134*, 12693−12699.
(3) (a) Krapp, A.; Pandey, K. K.; Frenking, G. *J. Am. Chem. Soc.* **2007**, *129*, 7596−7610. (b) Krapp, A.; Frenking, G. *J. Am. Chem. Soc.* **2008**, *130*, 16646−16658. (c) Comas-Vives, A.; Harvey, J. N. *Eur. J. Inorg. Chem.* **2011**, 5025−5035.
(4) (a) Royo, B.; Peris, E. *Eur. J. Inorg. Chem.* **2012**, *2012*, 1309−1318. (b) López, L. A.; Barrio, P.; Borge, J. *Organometallics* **2012**, *31*, 7844−7848. (c) Hildebrandt, B.; Raub, S.; Frank, W.; Ganter, C. *Chem.—Eur. J.* **2012**, *18*, 6670−6678. (d) Donnelly, K. F.; Petronilho, A.; Albrecht, M. *Chem. Commun.* **2013**, DOI: 10.1039/C2CC37881G.
(5) Penka, E. F.; Schlapfer, C. W.; Atanasov, M.; Albrecht, M.; Daul, C. *J. Organomet. Chem.* **2007**, *692*, 5709−5716.
(6) (a) Tonner, R.; Frenking, G. *Chem.—Eur. J.* **2008**, *14*, 3260−3272. (b) Tonner, R.; Frenking, G. *Chem.—Eur. J.* **2008**, *14*, 3273−3289. (c) Patel, D. S.; Bharatam, P. V. *J. Phys. Chem. A* **2011**, *115*, 7645−7655. (d) Patel, D. S.; Bharatam, P. V. *Chem. Commun.* **2009**, 1064−1066. (e) Bhatia, S.; Bagul, C.; Kasetti, Y.; Patel, D. S.; Bharatam, P. V. *J. Phys. Chem. A* **2012**, *116*, 9071−9079.
(7) (a) Conradie, J.; Ghosh, A. *Inorg. Chem.* **2010**, *49*, 243−248. (b) Li, Y.; Huang, J. S.; Zhou, Z. Y.; Che, C. M.; You, X. Z. *J. Am. Chem. Soc.* **2002**, *124*, 13185−13193. (c) Goodrich, L. E.; Paulat, F.; Praneeth, V. K. K.; Lehnert, N. *Inorg. Chem.* **2010**, *49*, 6293−6316. (d) Halder, P.; Dey, A.; Paine, T. K. *Inorg. Chem.* **2009**, *48*, 11501−11503. (e) Li, Y.; Huang, S.-H.; Zhou, Z.-Y.; Che, C.-M. *Chem. Commun.* **2003**, 1362−1363. (f) Ho, C.-M.; Zhang, J.-L.; Zhou, C.-Y.; Chan, O.-Y.; Yan, J.-J.; Zhang, F.-Y.; Huang, J.-S.; Che, C.-M. *J. Am. Chem. Soc.* **2010**, *132*, 1886−1894. (g) Deng, Q.-H.; Chen, J.; Huang, J.-S.; Chui, S. S.-Y.; Zhu, N.; Li, G.-Y.; Che, C.-M. *Chem.—Eur. J.* **2009**, *15*, 10707−10712. (h) Maux, P. L.; Roisnel, T.; Nicolas, I.; Simonneaux, G. *Organometallics* **2008**, *27*, 3037−3042.
(8) (a) Di Rocco, D. A.; Oberg, K. M.; Rovis, T. *J. Am. Chem. Soc.* **2012**, *134*, 6143−6145. (b) DeTar, D. F.; Westheimer, F. H. *J. Am. Chem. Soc.* **1959**, *81*, 175−178. (c) Breslow, R. *J. Am. Chem. Soc.* **1958**, *80*, 3719−3726. (d) Nyce, G. W.; Glauser, T.; Connor, E. F.; Möck, A.; Waymouth, R. M.; Hedrick, J. L. *J. Am. Chem. Soc.* **2003**, *125*, 3046−3056.
(9) (a) Gautier, A.; Cisnetti, F. *Metallomics* **2012**, *4*, 23−32. (b) Hindi, K.; Sicilianom, T.; Durmus, S.; Panzner, M.; Medvetz, D.; Reddy, V.; Hogue, L.; Hovis, C.; Hilliard, J.; Mallett, R.; Tessier, C.; Cannon, C.; Youngs, W. *J. Med. Chem.* **2008**, *51*, 1577−1583. (c) Hindi, K. M.; Panzner, M. J.; Tessier, C. A.; Cannon, C. L.; Youngs, W. J. *Chem. Rev.* **2009**, *109*, 3859−3884. (d) Melaiye, A.; Simons, R. S.; Milsted, A.; Pingitore, F.; Wesdemiotis, C.; Tessier, C. A.; Youngs, W. J. *J. Med. Chem.* **2004**, *47*, 973−977.
(10) (a) Orr, S. T. M.; Ripp, S. L.; Ballard, T. E.; Henderson, J. L.; Scott, D. O.; Obach, R. S.; Sun, H.; Kalgutkar, A. S. *J. Med. Chem.* **2012**, *55*, 4896−4933. (b) *Cytochrome P450: Structure, Mechanism, and Biochemistry*; de Montellano, P. R. O., Correia, M. A., Kluwer Academic/ Plenum Press: New York, 2005; pp 247−322.
(11) (a) Murray, M. *J. Toxicol. Environ. Health, Part B* **2012**, *15*, 365−395. (b) Murray, M. *Curr. Drug. Metab.* **2000**, *1*, 67−84.
(12) (a) Pentyala, S.; Rahman, A.; Mishra, S.; Muthiki, S.; Hughes, E.; Bikkani, A.; Cervo, K.; Maruso, C.; Khan, S. *Int. J. Med. Med. Sci.* **2011**, *3*, 22−31. (b) Zhao, S. X.; Dalvie, D. K.; Kelly, J. M.; Soglia, J. R.; Frederick, K. S.; Smith, E. B.; Obach, S.; Kalgutkar, A. S. *Chem. Res. Toxicol.* **2007**, *20*, 1649−1657.
(13) (a) Bertelsen, K. M.; Venkatakrishnan, K.; Von Moltke, L. L.; Obach, R. S.; Greenblatt, D. J. *Drug Metab. Dispos.* **2003**, *31*, 289−293. (b) Hemeryck, A.; Belpaire, F. M. *Curr. Drug Metab.* **2002**, *3*, 13−37. (c) Venkatakrishnan, K.; Obach, R. S. *Drug Metab. Dispos.* **2005**, *33*, 845−852. (d) Bloomer, J. C.; Woods, F. R.; Haddock, R. E.; Lennard, M. S.; Tucker, G. T. *Br. J. Clin. Pharmacol.* **1992**, *33*, 521−523.
(14) Gasbarrini, G.; Gentiloni, N.; Febbraro, S.; Gasbarrini, A.; Di Campli, C.; Cesana, M.; Miglio, F.; Miglioli, M.; Ghinelli, F.; D'Ambrosi, A.; Amoroso, P.; Pacini, F.; Salvadori, G. *J. Hepatol.* **1997**, *27*, 583−586.
(15) (a) Mesnil, M.; Testa, B.; Jenner, P. *Xenobiotica* **1988**, *18*, 1097−1106. (b) Zhang, K.; Lepage, F.; Cuvier, G.; Astoin, J.; Rashed, M. S.; Baillie, T. A. *Drug Metab. Dispos.* **1990**, *18*, 794−803. (c) Tran, A.; Rey, E.; Pons, G.; Rousseau, M.; d'Athis, P.; Olive, G.; Mather, G. G.; Bishop, F. E.; Wurden, C. J.; Labroo, R.; Trager, W. F.; Kunze, K. L.; Thummel, K. E.; Vincent, J. C.; Gillardin, J. M.; Lepage, F.; Levy, R. H. *Clin. Pharmacol. Ther.* **1997**, *62*, 490−504.
(16) Nishikibe, M.; Ohta, H.; Okada, M.; Ishikawa, K.; Hayama, T.; Fukuroda, T.; Noguchi, K.; Saito, M.; Kanoh, T.; Ozaki, S.; Kamei, T.; Hara, K.; William, D.; Kivlighn, S.; Krause, S.; Gabel, R.; Zingaro, G.; Nolan, N.; O'Brien, J.; Clayton, F.; Lynch, J.; Pettibone, D.; Siegl, P. *J. Pharmacol. Exp. Ther.* **1999**, *289*, 1262−1270.
(17) Chiba, M.; Nishime, J. A.; Chen, I. W.; Vastag, K. J.; Sahly, Y. S.; Kim, B. M.; Dorsey, B. D.; Vacca, J. P.; Lin, J. H. *Biochem. Pharmacol.* **1998**, *56*, 223−230.
(18) Subehan, U. T.; Kadota, S.; Tezuka, Y. *Planta Med.* **2006**, *72*, 527−532.
(19) (a) Yasuda, K.; Ikushiro, S.; Wakayama, S.; Itoh, T.; Yamamoto, K.; Kamakura, K.; Munetsuna, E.; Ohta, M.; Sakaki, T. *Drug Metab. Dispos.* **2012**, *40*, 1917−26. (b) Yasuda, K.; Sakaki, T. *Expert Opin. Drug Metab. Toxicol.* **2012**, *8*, 93−102. (c) Jan, K.-C.; Wei, Y.; Chang, Hwang, L. S.; Ho, C.-T. *J. Agric. Food Chem.* **2012**, *60*, 8616−8623. (d) Moazzami, A. A.; Andersson, R. E.; Kamal-Eldin, A. *J. Nutr.* **2007**, *137*, 940−944.
(20) (a) Julsing, M. K.; Vasilev, N. P.; Schneidman-Duhovny, D.; Muntendam, R.; Woerdenbag, H. J.; Quax, W. J.; Wolfson, H. J.; Ionkova, I.; Kayser, O. *Eur. J. Med. Chem.* **2008**, *43*, 1171−1179. (b) Usia, T.; Watabe, T.; Kadota, S.; Tezuka, Y. *Life Sci.* **2005**, *76*, 2381−2391.
(21) Salminen, K. A.; Meyer, A.; Imming, P.; Raunio, H. *Drug Metab. Dispos.* **2011**, *39*, 2283−2289.
(22) Keseru, G. M.; Kolossvary, I.; Szekely, I. *Int. J. Quantum Chem.* **1999**, *73*, 123−135.
(23) (a) Kent, U. M.; Jushchyshyn, M. I.; Hollenberg, P. F. *Curr. Drug Metab.* **2001**, *2*, 215−243.
(24) Kalgutkar, A. S.; Obach, R. S.; Maurer, T. S. *Curr. Drug Metab.* **2007**, *8*, 407−447.
(25) Fontana, E.; Dansette, P. M.; Poli, S. M. *Curr. Drug Metab.* **2005**, *6*, 413−454.
(26) Hollenberg, P. F.; Kent, U. M.; Bumpus, N. N. *Chem. Res. Toxicol.* **2008**, *21*, 189−205.
(27) Hanson, K. L.; Van den Brink, B. M.; Babu, K. N.; Allen, K. E.; Nelson, W. L.; Kunze, K. L. *Drug Metab. Dispos.* **2010**, *38*, 963−972.
(28) Taxak, N.; Desai, P. V.; Patel, B.; Mohutsky, M.; Klimkowski, V. J.; Gombar, V.; Bharatam, P. V. *J. Comput. Chem.* **2012**, *33*, 1740−1747.
(29) (a) Pandey, G.; Balakrishnan, M. *J. Org. Chem.* **2008**, *73*, 8128−8131. (b) Pandey, G.; Balakrishnan, M.; Swaroop, P. S. *Eur. J. Org. Chem.* **2008**, 5839−5847. (c) Pandey, G.; Murugan, A.; Balakrishnan, M. *Chem. Commun.* **2002**, *6*, 624−625. (d) Collins, J.; Rinner, U.; Moser, M.; Hudlicky, T. *J. Org. Chem.* **2010**, *75*, 3069−3084. (e) Fatima, S.; Sharma, A.; Saxena, R.; Tripathi, R.; Shukla, S. K.; Pandey, S. K.; Tripathi, R.; Tripathi, R. P. E. *J. Med. Chem.* **2012**, *55*, 195−204. (f) McNultya, J.; Naira, J. J.; Singh, M.; Crankshaw, D. J.; Holloway, A. C. *Bioorg. Med. Chem. Lett.* **2010**, *20*, 2335−2339. (g) Nair, J. J.; Rárová, L.; Strna, M.; Bastida, J.; Stade, J. V. *Bioorg. Med. Chem. Lett.* **2012**, *22*, 6195−6199. (h) Prashanth, M. K.; Revanasiddappa, H. D.; Rai, K. M. L.; Veeresh, B. *Bioorg. Med. Chem. Lett.* **2012**, *22*, 7065−7070.
(30) Parr, R. G. *Density Functional Theory of Atoms and Molecules*; Oxford University Press: New York, 1989; pp 1−325.
(31) Frisch, M. J.; Trucks, G. W.; Schlegel, H. B.; Scuseria, G. E.; Robb, M. A.; Cheeseman, J. R.; Montgomery, J. A., Jr.; Vreven, T.; Kudin, K. N.; Burant, J. C.; Millam, J. M.; Bakken, V.; Adamo, C.; Jaramillo, J.; Gomperts, R.; Scuseria, G. E.; Stratmann, R. E.; Yazyev, O.; Austin, A. J.; Cammi, R.; Pomelli, C.; Iyengar, S. S.; Ochterski, J. W.; Ayala, P. Y.; Morokuma, K.; Voth, G. A.; Salvador, P.; Robb, M.

A.; Dannenberg, J. J.; Zakrzewski, V. G.; Dapprich, S.; Daniels, A. D.; Tomasi, J.; Strain, M. C.; Farkas, O.; Malick, D. K.; Rabuck, A. D.; Raghavachari, K.; Foresman, J. B.; Cheeseman, J. R.; Ortiz, J. V.; Cui, Q.; Baboul, A. G.; Barone, V.; Clifford, S.; Cioslowski, J.; Stefanov, B. B.; Liu, G.; Liashenko, A.; Piskorz, P.; Komaromi, I.; Montgomery, J. A., Jr.; Martin, R. L.; Fox, D. J.; Mennucci, B.; Keith, T.; Al-Laham, M. A.; Peng, C. Y.; Nanayakkara, A.; Challacombe, M.; Gill, P. M. W.; Johnson, B.; Chen, W.; Vreven, T.; Wong, M. W.; Cossi, M.; Gonzalez, C.; Pople, J. A.; Kudin, K. N.; Scalmani, G. *Gaussian 03, revision C.02*; Gaussian, Inc.: Wallingford, CT, 2004.

(32) (a) Becke, A. D. *J. Chem. Phys.* **1993**, *98*, 5648−5652. (b) Becke, A. D. *J. Chem. Phys.* **1993**, *98*, 1372−1377. (b) Lee, C. T.; Yang, W. T.; Parr, R. G. *Phys. Rev. B: Condens. Matter Mater. Phys.* **1988**, *37*, 785−789.

(33) (a) Chen, Z.; Wannere, C. S.; Corminboeuf, C.; Puchta, R.; Schleyer, P. v. R. *Chem. Rev.* **2005**, *105*, 3842−3888. (b) Woodcock, H. L.; Moran, D.; Brooks, B. R.; Schleyer, P. v. R.; Schaefer, H. F., III. *J. Am. Chem. Soc.* **2001**, *123*, 4331−4335. (c) Bourissou, D.; Guerret, O.; Gabbai, F. P.; Bertrand, G. *Chem. Rev.* **2000**, *100*, 39−92. (d) Nyulaszi, L.; Veszpremi, T.; Forro, A. *Phys. Chem. Chem. Phys.* **2000**, *2*, 3127−3129.

(34) (a) Herrmann, W. A.; Köcher, C. *Angew. Chem., Int. Ed.* **1997**, *36*, 2162−2187. (b) Katari, M.; Rao, M. N.; Rajaraman, G.; Ghosh, P. *Inorg. Chem.* **2012**, *51*, 5593−5604. (c) Vyboishchikov, S. F.; Frenking, G. *Chem.—Eur. J.* **1998**, *4*, 1439−1448. (d) Ryan, S. J.; Stasch, A.; Paddon-Row, M. N.; Lupton, D. W. *J. Org. Chem.* **2012**, *77*, 1113−1124. (e) Holloczki, O.; Kelemen, Z.; Nyulaszi, L. *J. Org. Chem.* **2012**, *77*, 6014−6022. (f) Gronert, S.; Keeffe, J. R.; O'Ferrall, R. A. M. *J. Am. Chem. Soc.* **2011**, *133*, 13381−3389.

(35) (a) Foresman, J. B.; Frisch, A. E. *Exploring Chemistry with Electronic Structure Methods*; Gaussian, Inc.: Pittsburgh, PA, 1995. (b) Hehre, W. J.; Radom, L.; Schleyer, P. V. R.; Pople, J. A. *Ab Initio Molecular Orbital Theory*; Wiley: New York, 1986. (b) Hay, P. J.; Wadt, W. R. *J. Chem. Phys.* **1985**, *82*, 270−283.

(36) Scott, A. P.; Radom, L. *J. Phys. Chem.* **1996**, *100*, 16502−16513.

(37) Schaefer, A.; Huber, C.; Ahlrichs, R. J. *J. Chem. Phys.* **1994**, *100*, 5829−5835.

(38) (a) Tomasi, J.; Mennucci, B.; Cancès, E. *THEOCHEM* **1999**, *464*, 211−226. (b) Cancès, M. T.; Mennucci, B.; Tomasi, J. A. *J. Chem. Phys.* **1997**, *107*, 3032−3037. (c) Mennucci, B.; Tomasi, J. *J. Chem. Phys.* **1997**, *106*, 5151−5158. (d) Mennucci, B.; Cancès, E.; Tomasi, J. *J. Phys. Chem. B* **1997**, *101*, 10506−10517.

(39) (a) Hirao, H.; Cheong, Z. H.; Wang, X. *J. Phys. Chem. B* **2012**, *116*, 7787−7794. (b) Lia, D.; Wanga, Y.; Han, K. *Coord. Chem. Rev.* **2012**, *256*, 1137−1150. (c) Taxak, N.; Dixit, V. A.; Bharatam, P. V. *J. Phys. Chem. A* **2012**, *116*, 10441−10450. (d) de Visser, S. P. In *Advances in Inorganic Chemistry. Inorganic/Bioinorganic Reaction Mechanisms*; van Eldik, R., Ivanović-Burmazović, I., Eds.; Academic Press: London, U.K., 2012; *Vol. 64*, Chapter 1, pp 1−31. (e) de Visser, S. P. *J. Am. Chem. Soc.* **2010**, *132*, 1087−1097. (f) Shaik, S.; Cohen, S.; Wang, Y.; Chen, H.; Kumar, D.; Thiel, W. *Chem. Rev.* **2010**, *110*, 949−1017. (g) Porros, C. S.; Sutcliffe, M. J.; de Visser, S. P. *J. Phys. Chem. A* **2009**, *113*, 11635−11642. (h) Shaik, S.; Hirao, H.; Kumar, D. *Acc. Chem. Res.* **2007**, *40*, 532−542. (i) Hirao, H.; Kumar, D.; Thiel, W.; Shaik, S. *J. Am. Chem. Soc.* **2005**, *127*, 13007−13018.

(40) (a) de Visser, S. P. *J. Biocatal. Biotransform.* **2012**, *1*, 1−5. (b) Rydberg, P. *J. Chem. Theory Comput.* **2012**, *8*, 2706−2712. (c) Rydberg, P.; Olsen, L. *J. Chem. Theory Comput.* **2011**, *7*, 3399−3404. (d) Kumar, D.; Thiel, W.; de Visser, S. P. *J. Am. Chem. Soc.* **2011**, *133*, 3869−3882. (e) Shaik, S.; Kumar, D.; de Visser, S. P. *J. Am. Chem. Soc.* **2008**, *130*, 10128−10140. (f) Rydberg, P.; Ryde, U.; Olsen, L. *J. Chem. Theory Comput.* **2008**, *4*, 1369−1377. (g) Kumar, D.; de Visser, S. P.; Sharma, P. K.; Hirao, H.; Shaik, S. *Biochemistry* **2005**, *44*, 8148−8158. (h) Li, C.; Zhang, L.; Zhang, C.; Hirao, H.; Wu, W.; Shaik, S. *Angew. Chem., Int. Ed.* **2007**, *46*, 8168−8170.

(41) Reed, A. E.; Weinstock, R. B.; Weinhold, F. *J. Chem. Phys.* **1985**, *83*, 735−746.

(42) (a) Vignolle, J.; Cattoen, X.; Bourissou, D. *Chem. Rev.* **2009**, *109*, 3333−3384. (b) Albrecht, M. *Science* **2009**, *326*, 532−533. (b) Woodcock, H. L.; Moran, D.; Brooks, B. R.; Schleyer, P. v. R.; Schaefer, H. F., III. *J. Am. Chem. Soc.* **2007**, *129*, 3763−3770. (d) Arduengo, A. J. *Acc. Chem. Res.* **1999**, *32*, 913−921. (e) Fischer, E. O.; Maasböl, A. *Angew. Chem., Int. Ed.* **1964**, *3*, 580−581.

(43) (a) Jonas, V.; Boehme, M.; Frenking, G. *J. Phys. Chem.* **1992**, *96*, 1640−1648. (b) Sidiropoulos, A.; Jones, C.; Stasch, A.; Klein, S.; Frenking, G. *Angew. Chem., Int. Ed.* **2009**, *48*, 9701−9704. (c) Nemcsok, D.; Wichmann, K.; Frenking, G. *Organometallics* **2004**, *23*, 3640−3646. (d) Boehme, C.; Frenking, G. *Organometallics* **1998**, *17*, 5801−5809. (e) Doddi, A.; Gemel, C.; Winter, M.; Fischer, R. A.; Goedecke, C.; Rzepa, H. S.; Frenking, G. *Angew. Chem., Int. Ed.* **2012**, DOI: 10.1002/anie.201204440. (f) Mück, L. A.; Timoshkin, A. Y.; Frenking, G. *Inorg. Chem.* **2012**, *51*, 640−646.

(44) (a) Ho, J.; Coote, M. L. *Wiley Interdiscip. Rev.: Comput. Mol. Sci.* **2011**, *1*, 649−660. (b) Moser, A.; Range, K.; York, D. M. *J. Phys. Chem. B* **2010**, *114*, 13911−13921.

(45) Yanai, T. K.; Mori, S. *Chem.—Eur. J.* **2009**, *15*, 4464−4473.

(46) (a) Tahsini, L.; Bagherzadeh, M.; Nam, W.; de Visser, S. P. *Inorg. Chem.* **2009**, *48*, 6661−6669. (b) Jeong, Y. J.; Kang, Y.; Han, A.-R.; Lee, Y.-M.; Kotani, H.; Fukuzumi, S.; Nam, W. *Angew. Chem., Int. Ed.* **2008**, *47*, 7321−7324.

(47) (a) Shaik, S.; de Visser, S. P.; Ogliaro, F.; Schwarz, H.; Schröder, D. *Curr. Opin. Chem. Biol.* **2002**, *6*, 556−567. (b) de Visser, S. P.; Kumar, D.; Cohen, S.; Shacham, R.; Shaik, S. *J. Am. Chem. Soc.* **2004**, *126*, 8362−8363.

(48) Balding, P. R.; Porro, C. S.; McLean, K. J.; Sutcliffe, M. J.; Maréchal, J. D.; Munro, A. W.; de Visser, S. P. *J. Phys. Chem. A* **2008**, *112*, 12911−12918.

(49) deVisser, S. P.; Shaik, S. *J. Am. Chem. Soc.* **2003**, *125*, 7413−7424.